Microscopic model analysis of ^{11}Li + p elastic scattering at 62, 68.4, and 75 MeV/nucleon

M. Y. M. Hassan,[1] M. Y. H. Farag,[1] E. H. Esmael,[1] and H. M. Maridi[1,2]
[1]*Physics Department, Faculty of Science, Cairo University, Cairo, Egypt*
[2]*National Atomic Energy Commission, Sana'a, Yemen*
(Received 17 July 2008; revised manuscript received 6 December 2008; published 28 January 2009)

^{11}Li + p elastic scattering data at three energies, 62, 68.4, and 75 MeV/nucleon, are analyzed with density-dependent M3Y and KH effective nucleon-nucleon (NN) interactions in the framework of the single folding model. The parameters of the density-dependent term are adjusted to fulfill saturation of nuclear matter. The optical potentials (OP's) and cross sections are calculated using four model densities of ^{11}Li, G (one-parameter Gaussian), GG (Gaussian-Gaussian), GO (Gaussian- oscillator), and the COSMA (cluster orbital shell model approximation). Comparative studies are performed for real, imaginary, and spin-orbit potentials with the phenomenological and microscopic forms. The microscopic volume and surface imaginary potentials are constructed from both the renormalized folded potentials and their derivatives. The sensitivity of the differential cross section to the four densities is tested. It is found that the ^{11}Li + p elastic scattering cross sections depend strongly upon the behavior of the corresponding potentials. The GG and GO densities obtained from analyzing the data, using Glauber multiple scattering theory at high energies, give good results at energies below 100 MeV/nucleon in the framework of the folding model. The OP's calculated in the microscopic form using few parameters give good agreement with the data. Thus, it is not necessary to introduce a large number of arbitrary fitting parameters as done in the phenomenological and semimicroscopic OP's. The KH effective interaction successfully describes ^{11}Li + p elastic scattering as the popular M3Y interaction. The obtained results of the reaction cross section are in good agreement with previous calculations.

DOI: 10.1103/PhysRevC.79.014612 PACS number(s): 21.10.Gv, 25.40.Cm, 25.60.Bx

I. INTRODUCTION

The ^{11}Li nucleus is a neutron-rich radioactive nucleus, which is assumed to be composed of core (^{9}Li) plus two neutrons in the p orbital state at large distance. The dineutron has a small separation energy of 0.247 MeV [1], so it is extremely loosely bound to the ^{9}Li core. The ^{11}Li has a long tail in its wave function leading to the so-called halo structures [1,2]. The halo of the nucleus extends its matter distribution to a large radius. The ^{11}Li nucleus is so short lived that it cannot be used as a target. Instead, direct reactions with a radioactive nuclear beam can be performed in inverse kinematics, where the role of the beam and target are interchanged. To understand the formation of a halo around the core of radioactive nuclei, it is useful to study the differential and reaction cross sections of the proton elastic scattering on exotic nuclei in inverse kinematics. ^{11}Li + p elastic scattering angular distributions were measured at intermediate incident energies, 62 [3], 68.4 [4], and 75 MeV/nucleon [5]. These distributions were then studied using different phenomenological and microscopic optical potential models (see, e.g., Refs. [3,5–18]).

The elastic scattering cross sections of ^{11}Li + p at 62 MeV/nucleon have been measured and analyzed using a phenomenological optical potential model [3], the best fit with experimental data was obtained with a combination of a shallow real potential and an imaginary potential with a long tail. Kanungo and Samanta [7] studied this reaction at 62, 68.4, and 75 MeV/nucleon and concluded that the phenomenological form of the potential gives a generalized description and does not include explicitly any structure information of the interacting nuclei.

At an incident energy range of 62–75 MeV/nucleon, the eikonal approach using proton and neutron density distributions has been used [5,8,13–15]. In Ref. [13], the eikonal and adiabatic approximations were employed to derive the optical potential that includes the breakup effect of halo neutrons to continuum states; it was shown that both the breakup of ^{11}Li and the exchange force of the p-n interaction are important to obtaining a good agrement with experimental data. Also in Ref. [15], it was found that the breakup effect of halo neutrons is essential to understanding the ^{11}Li + p elastic scattering cross sections at 62 MeV/nucleon.

The Glauber multiple scattering theory has been used to study charge and matter distributions from the measured ^{11}Li + p elastic scattering cross sections at high energies near energy 700 MeV/nucleon [16,17]. These studies found that the densities that do not distinguish between neutrons and protons, i.e., where the nucleus is taken as a whole such as one-parameter Gaussian (G) and symmetrized Fermi (SF) densities, failed to describe the data. Whereas the densities that assume the nucleus to consist of core (^{9}Li) and halo (two neutrons) with different spatial distributions, such as Gaussian-Gaussian (GG) and Gaussian-oscillator (GO), give good descriptions of the data.

Crespo *et al.* [10,19] evaluated ^{11}Li elastic scattering at 62 and 800 MeV/nucleon using the optical model of both the single scattering approximation to mean field Kerman-McManus-Thaler (KMT) [20] and the few-body multiple scattering expansion of the total transition amplitude (MST) [21]. They found that the calculated elastic scattering observable may not be very sensitive to details of the structure input but depends on the scattering theory.

A successful tool for the analysis of the elastic scattering data at relatively low incident energies is the folding model. The basic inputs to folding calculations are the effective nucleon-nucleon (NN) interaction and the nuclear densities. The calculation of OP's using the folding approach for $^{11}\mathrm{Li}+p$ elastic scattering has been considered in Refs. [6,7,9,11,12]. The real part of the OP's of $^{11}\mathrm{Li}+p$ elastic scattering have been calculated in the framework of the single folding model using the density-independent M3Y [7,12]; the isospin-, density-, and momentum-dependent modified Seyler-Blanchard (SBM) [6,7]; and the Jeukenne, Lejeune, and Mahaux (JLM) effective NN interactions [9]. $^{11}\mathrm{Li}+p$ elastic differential cross sections at 62 MeV/nucleon have been calculated using the M3Y-Reid effective NN interaction by Chaudhari [12]. He used the harmonic oscillator density for ^{9}Li and determined the density of the two halo neutrons by Fourier-Bessel analysis. This density gives a good description of the elastic scattering data. Kanungo and Samanta studied this reaction at 62, 68.4, and 75 MeV/nucleon using the density independent M3Y-Reid and SBM effective NN interactions with two densities [7], the first is composed of a harmonic oscillator (HO) density of a core and Gaussian density of two halo neutrons, and the second is the cluster orbital shell model (COSM) which mixes many j orbits [22]. The same reaction has been studied using the SBM effective NN interaction which was folded with the COSM density [6] and the JLM interaction with Hartree-Fock densities [9]. These studies found that the real part of folded $^{11}\mathrm{Li}+p$ potentials needs a reduction factor indicating the possible effect of a strong breakup channel [6,7,9].

In the present work, the real part of the OP is calculated in the framework of the single folding model using two different types of density-dependent effective NN interactions, namely, M3Y and Knyazkov and Hefter (KH), with four different forms of ^{11}Li density distributions at 62, 68.4, and 75 MeV/nucleon. The elastic scattering data are analyzed in microscopic and semimicroscopic analyses. The density-dependent term, whose parameters are adjusted to fulfill saturation of nuclear matter, is introduced [23]. The effect of different nucleon-nucleon interactions is studied. In addition, the ability of the four different target densities to describe the nuclear reaction considered is tested. Also, the role of the spin-orbit term is discussed. The imaginary part of the OP is studied with phenomenological and microscopic forms. One of the aims of the present work is to calculate $^{11}\mathrm{Li}+p$ elastic scattering cross sections that describe the experimental data using a minimal number of fitting parameters. The detailed formalism is given in Sec. II. The results and calculations are presented in Sec. III, while the discussion and conclusions are given in Sec. IV.

II. FORMALISM

A. Folded potential

The nucleon-nucleus potential can be obtained by single folding the density distribution of the nucleus with the nucleon-nucleon effective interaction [24]

$$V_F(r) = \int \rho(\acute{\mathbf{r}})\nu_{nn}(s)\,d\acute{\mathbf{r}}, \tag{1}$$

where $s = |\mathbf{r} - \acute{\mathbf{r}}|$ is the distance between the two nucleons, $\rho(\acute{\mathrm{r}})$ is the density of the nucleus at r, and $\nu_{nn}(s)$ is the effective NN interaction between two nucleons.

B. Nucleon-nucleon effective interactions

The effective NN interaction is taken in two forms: M3Y and Knyazkov and Hefter (KH) interactions.

1. M3Y interaction

The popular M3Y potential derived by Bertsch *et al.* [25] was obtained from the fitting of the G-matrix element of the Reid-Elliot NN interaction. The parametrized form of the M3Y interaction introduced by Satchler and Love [24] is

$$\nu_{nn}(s) = 7999\frac{\exp(-4s)}{4s} - 2134\frac{\exp(-2.5s)}{2.5s} + J_{00}(E)\delta(s), \tag{2}$$

where s is the distance between the two nucleons. The term $J_{00}(E)\delta(s)$ is the zero-range pseudopotential with the knock-on strength $J_{00}(E)$, which depends weakly on the bombarding energy E and is given by

$$J_{00}(E) = -276(1 - 0.005E/A)\ \mathrm{MeV\,fm^3}, \tag{3}$$

where E is the incident energy and A the mass number of the projectile. Taking into consideration the density-dependent effect, the NN interaction $\nu_{nn}(s)$ in Eq. (2) is given by $\nu_{nn}(s,\rho)$ as

$$\nu_{nn}(s,\rho) = \nu_{nn}(s)F(\rho), \tag{4}$$

where $F(\rho)$ is the density-dependent factor and is given as [23,26]

$$F(\rho) = c(1 - \beta\rho), \tag{5}$$

where c and β are the parameters of the density-dependent factor. The M3Y NN interaction with this density-dependent term $F(\rho)$ is labeled as BDM3Y1 [26].

2. Knyazkov and Hefter (KH) interaction

Knyazkov and Hefter considered the effective NN interaction in the form [27]

$$\nu_{nn}(s) = \sum_{k=1}^{2} \nu_k \exp\left(-s^2/a_k^2\right) + J_{00}(E)\delta(s), \tag{6}$$

where the parameters ν_k and a_k are taken from Ref. [27] and given in Table I. The KH Gaussian effective NN interaction has been used to successfully construct an OP to reproduce the elastic scattering cross section (see, e.g., Ref. [28]). Also, the

TABLE I. Parameters of KH interaction.

a_1 (fm)	a_2 (fm)	ν_1 (MeV)	ν_2 (MeV)
0.8	0.5	−601.99	2256.4

density-dependent term is introduced into the KH interaction as in the M3Y interaction.

C. Nuclear matter calculations

The two parameters c and β in the density-dependent factor $F(\rho)$ in Eq. (5) have been fitted to reproduce the saturation conditions [23]

$$\rho_0 = 0.17 \text{ fm}^{-3}, \quad (E/A)_{\rho=\rho_0} = -16.0 \text{ MeV}, \\ \frac{\partial}{\partial\rho}(E/A)_{\rho=\rho_0} = 0. \tag{7}$$

The energy per nucleon $\epsilon = E/A$ is obtained using the effective NN interaction $v_{nn}(s)$ for the spin and isospin symmetric cold infinite nuclear matter and is given by [23]

$$\epsilon = \frac{3\hbar^2 k_f^2}{10m} + F(\rho)\rho\frac{J_v}{2}, \tag{8}$$

where m is the nucleon mass, and the Fermi momentum k_f is given by

$$k_f^3 = \tfrac{3}{2}\pi^2\rho. \tag{9}$$

ρ is the nucleon density while ρ_0 is the saturation density for the spin and isospin symmetric cold infinite nuclear matter, and J_v represents the volume integral of the NN interaction supplemented by the zero-range pseudopotential having the form

$$J_v = \int v_{nn}(s)\, d^3s. \tag{10}$$

The density-dependent parameters c and β are obtained from Ref. [23] by

$$\beta = \frac{1-p}{\rho(4-2p)}, \tag{11}$$

and

$$c = -\frac{2\hbar^2 k_{f_0}^2}{5mJ_v\rho_0(1-2\beta\rho_0)}, \tag{12}$$

where

$$p = \frac{10m\epsilon_0}{\hbar^2 k_{f_0}^2}, \tag{13}$$

and

$$k_{f_0} = \left(\frac{3}{2}\pi^2\rho_0\right)^{1/3}. \tag{14}$$

The incompressibility K_0 of the spin and isospin symmetric cold infinite nuclear matter is given by [23]

$$K_0 = -\frac{3\hbar^2 k_{f_0}^2}{5m} - 9J_v c\beta\rho_0^2. \tag{15}$$

The obtained parameters of density dependence, c and β, and the incompressibility K_0 are listed in Table II.

TABLE II. Incompressibility and parameters of density-dependent part $F(\rho) = c(1-\beta\rho)$ for M3Y and KH NN effective interactions at saturation conditions.

Interaction	β (fm^2)	c	K_0 (MeV)
M3Y-Reid	2.2185	1.6674	380.755
KH	2.2185	1.6679	380.755

D. Nuclear density distributions

The ^{11}Li nucleus is assumed to be composed of a ^{9}Li core and dineutron cluster [2]. Thus the density distribution of ^{11}Li nucleus can be written as

$$\rho_{^{11}\text{Li}} = \rho_{^9\text{Li}} + \rho_{2n}. \tag{16}$$

The rms radius of ^{11}Li is quite large compared to that of ^{9}Li, and ^{11}Li is known to be a Borromean nucleus [29], which is a three-body system that falls apart when one of the particles is removed [30]. The deduced core size of ^{11}Li slightly exceeds the measured radius of ^{9}Li, which is assumed to be the core in ^{11}Li. This may be explained by the fact that the motion of the center of mass of the core around the center of mass of the whole nucleus increases the effective core size. Also, this may be due to the core polarization [17].

Different matter density distributions have been obtained from the measured ^{11}Li + p elastic scattering cross sections at high incident energy using the Glauber multiple scattering theory [16,17,31]. It is found that the densities that do not distinguish between neutrons and protons fail to describe the data, while the densities that assume the nucleus to consist of core (^{9}Li) and halo (two neutrons) with different spatial distributions give good descriptions of the data.

To test the sensitivity to the radial shape of the nuclear matter distribution, four different nuclear matter density distributions are considered in the present work.

1. One-parameter Gaussian (G) density

The one-parameter Gaussian density does not make a difference between core and valence nucleons, it is given as

$$\rho(r) = A\rho_0 \exp\left(-\frac{r^2}{b^2}\right), \tag{17}$$

where, A is the mass number of the ^{11}Li nucleus, $\rho_0 = (1/\pi b^2)^{3/2}, b^2 = 2R_m^2/3$, and the rms radius of the ^{11}Li nucleus is $R_m = 3.10$ fm [32].

2. Gaussian-Gaussian (GG) density

In this type of density, the core (^{9}Li) and halo ($2n$) density distributions are described by Gaussian form [16,17,33]. The GG density can be written as

$$\rho(r) = N_c\rho_{0c}\exp\left(-\frac{r^2}{b_c^2}\right) + N_h\rho_{0h}\exp\left(-\frac{r^2}{b_h^2}\right), \tag{18}$$

where $\rho_{0j} = (1/\pi b_j^2)^{3/2}$ and $b_j^2 = 2R_j^2/3$ with $j = c, h$, and R_c and R_h denote the rms radii of the core and halo nucleon

distributions ρ_c and ρ_h, respectively. N_c and N_h are the number of nucleons in the core and halo, respectively, and are given as $N_c = 9$ and $N_h = 2$ for ^{11}Li nucleus. The matter radius is given by [33]

$$R_m = \left[\frac{9R_c^2 + 2R_h^2}{11}\right]^{1/2}. \quad (19)$$

R_c and R_h are given in Ref. [17] as $R_c = 2.56$, $R_h = 6.31$, and $R_m = 3.55$ fm.

3. The Gaussian-oscillator (GO) density

Here the core density distribution is a Gaussian as in Eq. (18), while the two valence neutrons are assumed to have a $1p$-shell harmonic oscillator distribution [10,31,33], that is,

$$\rho(r) = N_c\rho_{0c}\exp\left(-\frac{r^2}{b_c^2}\right) + N_h\rho_{0h}\left(\frac{r^2}{b_h^2}\right)\exp\left(-\frac{r^2}{b_h^2}\right), \quad (20)$$

where, ρ_{0c} and b_c^2 are as in Eq. (18), $\rho_{0h} = (2/3)(1/\pi b_h^2)^{3/2}$, and $b_h^2 = 2R_h^2/5$; also, $N_c = 9$ and $N_h = 2$ for the ^{11}Li nucleus. The values of R_c and R_h are given in Ref. [17] as $R_c = 2.50$, $R_h = 5.86$, and $R_m = 3.37$ fm.

4. Cluster orbital shell model approximation (COSMA) density

In the COSMA density, the valence neutron density is taken for four extreme cases, in which the valence neutrons are in the $1p$, $2s$, $1d$, and $1s$ states [8,29]. These densities are given by the following formulas:

$$\rho^{1p} = \tfrac{2}{3}\rho_0 x^2\exp(-x^2), \quad (21)$$

$$\rho^{2s} = \tfrac{2}{3}\rho_0(x^2 - 1.5)^2\exp(-x^2), \quad (22)$$

$$\rho^{1d} = \tfrac{4}{15}\rho_0 x^4\exp(-x^2), \quad (23)$$

$$\rho^{1s} = \rho_0\exp(-x^2), \quad (24)$$

where $\rho_0 = (1/\pi b^2)^{3/2}$, $x = r/b$, and b corresponds to the radius of the nucleus. For the ^{11}Li nucleus, the two valence neutrons are put into a mixture of the $1p$ and $2s$ orbitals; this mixture allows one to reproduce the experimental data on transverse momentum distributions of ^{9}Li from fragmentation of ^{11}Li [29]. Then, the COSMA density of ^{11}Li is given by [8,29]

$$\rho_i(r) = N_{ci}\frac{\exp(-r^2/a^2)}{\pi^{3/2}a^3} + N_{vi}\frac{2\exp(-r^2/b^2)}{3\pi^{3/2}b^5} \times\left[Ar^2 + \frac{B}{b^2}\left(r^2 - \frac{3}{2}b^2\right)^2\right], \quad i = n, p, \quad (25)$$

where $N_{cp} = 3$, $N_{cn} = 6$, $N_{vp} = 0$, $N_{vn} = 2$, $a = 1.89$ fm, $b = 3.68$ fm, $A = 0.81$, $B = 0.19$, and $R_m = 3.21$ fm.

The shape of the different cases of the density distributions of ^{11}Li are shown in Fig. 1, in linear and logarithmic scale. One can see that COSMA density is the largest at distance ($r < 3$ fm), while the G density is the smallest one. For large r ($r > 6$ fm), the G density, which describes the nucleus as a whole, is the smallest because it does not have a tail, whereas the densities that are formed from a core and two valence neutrons have tails. The GO density has the longest tail, so it best describes the large radius of ^{11}Li.

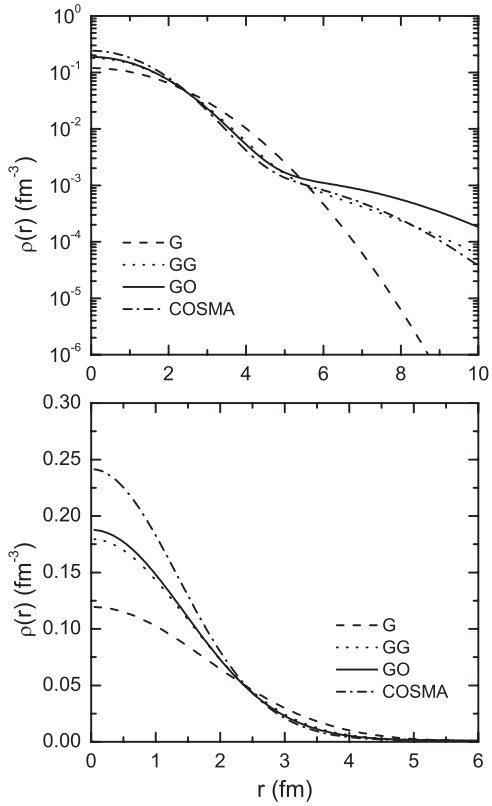

FIG. 1. Densities of ^{11}Li used in this work.

E. Method of calculation

We start with the calculation of $^{11}\text{Li} + p$ elastic cross sections using the real part of OP calculated within the single folding approach V_F; we introduce the renormalization factor N_R, while the other parts are given in the usual phenomenological form. The total optical potential can be written as

$$U_{\text{opt}}(r) = N_R V_F(r) + iW_I(r) + U_c(r) + U_{\text{so}}(r), \quad (26)$$

where N_R is the renormalization factor of the folded potential $V_F(r)$, W_I is the imaginary part, $U_c(r)$ is the Coulomb potential of a uniformly charged sphere of radius $1.29A^{1/3}$ [3], and U_{so} is the spin-orbit potential. The folded potentials using M3Y interaction are purely real, so the imaginary part is either constructed independently or, as done most frequently, treated phenomenologically [34,35]. They are independent of the density of the nuclear matter in which the two nucleons are embedded and also independent of energy except for the weak dependence of knock-on exchange [34,35].

In the present work, we use the imaginary potential with phenomenological and microscopic forms, so we introduce the renormalization factors N_{IV} and N_{IS} for the volume and surface imaginary microscopic potentials, respectively. To study the effect of these different forms of the imaginary parts, three types of OP's are considered:

(A) The phenomenological imaginary and spin-orbit potentials are used in the forms [6,7,36]

$$W_I(r) = -W_v f_v(r) + 4a_s W_s \frac{d}{dr} f_s(r), \tag{27}$$

and

$$U_{\rm so}(r) = \lambda_\pi^2 V_{\rm so} \frac{1}{r}\frac{d}{dr} f_{\rm so}(r)\mathbf{L}.\mathbf{S}, \tag{28}$$

where $f_x(r) = [1 + \exp(\frac{r-R_x}{a_x})]^{-1}$, $R_x = r_x A^{1/3}$, and $\lambda_\pi^2 = (\frac{\hbar}{2m_\pi c})^2 = 2$ fm^2. The subscripts $x = v, s$, and 'so' denote volume imaginary, surface imaginary, and spin orbit, respectively, and $W_v(W_s)$ and $V_{\rm so}$ are the strengths of the volume (surface) imaginary and the spin-orbit potentials. The parameters of the above parts of the optical potential are obtained after slight adjustment starting from the parameters of the phenomenological best fit at Ref. [12].

(B) In this case, the phenomenological volume imaginary part of the OP is replaced by a part of the folded potential, see Refs. [4,6]:

$$W_I(r) = N_{\rm IV} V_F(r) + 4a_s W_s \frac{d}{dr} f_s(r). \tag{29}$$

The phenomenological spin-orbit term is taken as in Eq. (28).

(C) Here, the derivative $(-r\frac{d}{dr}V_F)$ of the folded potential is added as the surface potential [37,38] as

$$W_I(r) = N_{\rm IV} V_F(r) + N_{\rm IS} r \frac{d}{dr} V_F(r). \tag{30}$$

The phenomenological spin-orbit term is again taken as in Eq. (28).

Let us denote the total ^{11}Li + p potential as M3Y-A, M3Y-B, and M3Y-C for potentials based upon the the real folded potential using the M3Y effective NN interaction, and the imaginary part of the optical potential is calculated with methods (A), (B), and (C), respectively. While the spin-orbit potential is taken phenomenologically as in Eq. (28). Similarly, we denote the potentials using the KH effective NN interaction as KH-A, KH-B, and KH-C.

To study the effect of spin-orbit potential with a different form from the standard form, $f_{\rm so}(r)$ in Eq. (28) is replaced by a microscopic real folding potential V_F. Then the spin-orbit term is taken as

$$U_{\rm so}(r) = N_{\rm so}\lambda_\pi^2 \frac{1}{r}\frac{d}{dr} V_F(r)\mathbf{L}.\mathbf{S}, \tag{31}$$

where the factor $N_{\rm so}$ corresponds to the strength $V_{\rm so}$.

A search on the renormalization factors and the phenomenological potential parameters are carried out to achieve minimum χ^2 given by [24]

$$\chi^2 = \frac{1}{N}\sum_{k=1}^{N}\left[\frac{\sigma_{\rm th}(\theta_k) - \sigma_{\rm ex}(\theta_k)}{\Delta\sigma_{\rm ex}(\theta_k)}\right]^2, \tag{32}$$

where $\sigma_{\rm th}(\theta_k)$ and $\sigma_{\rm ex}(\theta_k)$ are the theoretical and experimental cross sections, respectively, at angle θ_k, $\Delta\sigma_{\rm ex}(\theta_k)$ is the experimental error, and N is the number of data points. The experimental data of ^{11}Li + p elastic scattering cross sections and related errors are taken for 62 [3], 68.4 [4], and 75 MeV/nucleon [5].

The volume integrals and the rms radii of the folded ^{11}Li + p potentials are calculated for the two interactions and the four densities at the three energies; these are defined by [36]

$$J = \frac{4\pi}{A_P A_T}\int V_F(r) r^2 dr. \tag{33}$$

$$\langle r\rangle^{1/2} = \left[\frac{\int r^2 V_F(r) r^2 dr}{\int V_F(r) r^2\, dr}\right]^{1/2}. \tag{34}$$

III. RESULTS AND DISCUSSION

A. Real optical potentials

The real part of the optical ^{11}Li + p potentials are calculated using the single folding model [Eq. (1)] with the two effective NN interactions, M3Y and KH, and the four densities, G, GG, GO, and COSMA, at the three energies, 62, 68.4, and 75 MeV/nucleon. The results of these calculations at the energy 62 MeV/nucleon are shown in Fig. 2. They are given without the renormalization factor N_R (i.e., $N_R = 1$). It is seen that the depths of the potentials using M3Y and KH effective NN interactions are approximately similar to each other. It is seen that the potential using the COSMA density has a larger depth than that using the GG and GO densities, while the potential depth for the G density is shallower than that for other densities; this holds in a small distance ($r < 3$ fm). At a large distance, the folded potential using the G density falls more rapidly than the potentials using the other densities, which have longer ranges. This is due to the type of density used. The folded potentials at the two other energies (68.4 and 75 MeV/nucleon) have similar behavior as the folded potential at 62 MeV/nucleon but with different depths, where the depths of the potentials decrease with increasing the energy.

The respective volume integrals and rms radii of the folded optical potentials, using the two density-dependent effective NN interactions, M3Y and KH, for the G, GG, GO, and COSMA densities at the three energies 62, 68.4 and 75 MeV/nucleon, are listed in Table III. The volume integral of

TABLE III. Volume integrals and rms radii of the folded ^{11}Li + p potentials including in-medium effect at the four densities and the M3Y and KH interactions for the three energies studied.

Energy (MeV/nucleon)	Density	$-J$ (MeV fm^3)		$R_{\rm rms}$ (fm)	
		M3Y	KH	M3Y	KH
62	G	507.895	508.127	3.831	3.853
	GG	492.307	492.531	4.289	4.310
	GO	489.595	489.818	4.124	4.145
	COSMA	470.436	470.650	4.128	4.148
68.4	G	494.549	494.777	3.847	3.869
	GG	479.371	479.591	4.303	4.324
	GO	476.729	476.948	4.139	4.160
	COSMA	458.074	458.285	4.143	4.163
75	G	480.786	481.009	3.864	3.887
	GG	466.03	466.246	4.319	4.340
	GO	463.462	463.677	4.155	4.177
	COSMA	445.326	445.533	4.158	4.180

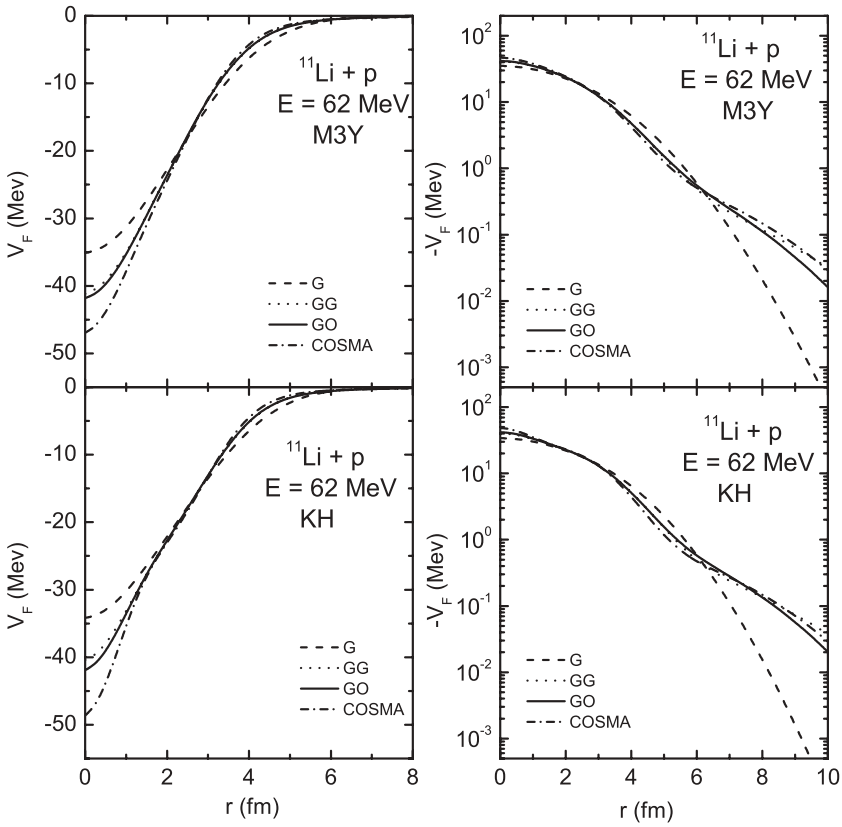

FIG. 2. Real folded ^{11}Li + p potentials with M3Y and KH interactions using G, GG, GO, and COSMA densities at energy $E =$ 62 MeV/nucleon.

the the real folded potential using the G density is larger than that for the other densities at the different energies while that using the COSMA density is the smallest one, this is due to the shape of the potential. The rms radius of the folding potential using the G density is the smallest one, because this density does not consider the halo structure. One can easily notice that the volume integrals decrease and the rms radii increase as the energy increases for all densities; this result is also found in Ref. [7]. One also notices that the volume integral and rms radius of the folded potential using M3Y and KH interactions have approximately the same behavior.

B. Effect of density distributions on the differential cross section

The differential cross sections of ^{11}Li + p elastic scattering at the three energies 62, 68.4, and 75 MeV/nucleon are calculated using M3Y-A and KH-A potentials (with real folded potential and phenomenological imaginary and spin-orbit potentials) for the four types of densities. The obtained results are shown in Fig. 3. The renormalization factors N_R, strength parameters of the phenomenological potentials which give good agreement with the experimental data, and total reaction cross sections for the four densities G, GG, GO, and COSMA, using the two effective NN interactions, M3Y and KH, at the three energies are listed in Table IV. The phenomenological imaginary and spin-orbit potentials are obtained after a slight enlargement starting with the parameters in Ref. [12]. To reduce the number of free parameters, the best radii and diffuseness parameters of volume and surface imaginary and spin-orbit phenomenological potentials are fixed at the three energies for all densities. These parameters are listed in Table V. One can see from Fig. 3 and the values of χ^2 from Table IV that the densities GG, GO, and COSMA, which allow for different distributions for the core and halo nucleons, give very good fitting with data, better than the G density. Then, the distribution form of two valence neutrons has a small effect on the obtained cross sections as mentioned in Refs. [17,33]. For the high energy around 700 MeV/nucleon [16,31], the cross section data of ^{11}Li + p elastic scattering using Glauber theory do not give a good description. However, in the present work, the G density gives acceptable fitting with data with our results in the framework of the single folding model at energies below 100 MeV/nucleon. The cross sections depend on the folded potential depths, where the differential cross section values increase as the potential depth decreases at the large angles ($\theta_{\text{c.m.}} > 40^\circ$), see Figs. 2 and 3. The GG and GO densities that were obtained from analyzing the measured ^{11}Li + p elastic scattering cross sections near energy 700 MeV/nucleon in the framework of Glauber multiple scattering theory [16,17,31] are used in the present work within the folding model at energies below 100 MeV/nucleon and give good results.

The renormalization factor N_R is found to be approximately the same for the two effective NN interactions M3Y and KH, and it decreases with increasing incident energy. These renormalization factors give an estimation of the $^{11}\text{Li} \rightarrow {}^{9}\text{Li} + 2n$ breakup channel effects on the elastic channel [6,7]; this is true for the stable isotopes ^{6,7}Li [6,24,37].

From Table IV, it is easily noted that with increasing incident energy, the strength of the spin-orbit potential V_{so} and the surface imaginary potential W_s are reduced. This is satisfied

TABLE IV. Renormalization factors N_R, strengths of the phenomenological potentials W_v, W_s, and V_{so}, and reaction cross sections σ_R obtained by fitting the elastic scattering data for ^{11}Li + p which were calculated using using M3Y-A and KH-A potentials with the four densities at the three energies studied.

Energy (MeV/nucleon)	Pot.	Case	N_R	W_v (MeV)	W_s (MeV)	V_{so} (MeV)	σ_R (mb)	χ^2
62	M3Y	G	0.61	13.7	3.7	9.9	367.2	2.95
		GG	0.64	12.9	3.7	9.5	359.3	0.85
		GO	0.65	13.2	3.7	9.6	362.2	0.75
		COSMA	0.63	13.5	3.7	9.8	363.8	0.70
	KH	G	0.62	12.7	3.7	9.3	355.7	4.13
		GG	0.64	12.7	3.7	8.9	351.0	1.52
		GO	0.65	12.7	3.7	8.9	353.1	1.18
		COSMA	0.63	12.7	3.7	9.1	353.7	0.88
68.4	M3Y	G	0.58	15.5	2.6	6.5	312.6	0.26
		GG	0.55	11.5	2.6	6.0	310.6	0.18
		GO	0.56	12.0	2.6	6.0	310.8	0.16
		COSMA	0.53	14.1	2.6	6.2	310.1	0.38
	KH	G	0.59	16.5	2.2	6.4	301.6	0.37
		GG	0.57	12.5	2.2	6.0	300.0	0.14
		GO	0.57	12.5	2.2	6.0	300.2	0.11
		COSMA	0.55	13.6	2.2	6.0	299.4	0.24
75	M3Y	G	0.56	8.7	1.5	5.9	201.3	0.97
		GG	0.53	7.0	1.5	5.5	200.5	0.17
		GO	0.54	7.2	1.5	5.5	200.7	0.14
		COSMA	0.51	7.9	1.5	5.5	200.5	0.15
	KH	G	0.56	8.0	1.2	5.8	185.1	1.24
		GG	0.54	6.5	1.2	5.4	184.6	0.30
		GO	0.55	7.0	1.2	5.4	184.6	0.28
		COSMA	0.52	7.5	1.2	5.5	184.4	0.16

for both M3Y and KH interactions. Also, we note that the spin-orbit strength depends somewhat on the renormalization factor of real OP (N_R increases with increasing V_{so}).

One can find that the change of the value of the total reaction cross section σ_R for the different densities used does not exceed 3%. Also, the total reaction cross section decreases with increasing projectile incident energy; this is agrees with that found in Ref. [7].

C. Comparative study between M3Y and KH interactions

A comparison between the phenomenological and microscopic real potentials and their corresponding differential cross sections is presented in Fig. 4. The real ^{11}Li + p optical potentials at 62 MeV/nucleon using Woods-Saxon form, whose parameters are given in Ref. [3], and the folding potentials (with renormalization factor $N_R = 0.65$) using M3Y and KH interactions with GO density are shown in Figs. 4(a) and 4(b). One can see that the Woods-Saxon potential is shallower (at small distance) than the two folded potentials using density-dependent M3Y and KH interactions which have similar behavior and have longer ranges than the phenomenological potential. Figure 4(c) presents the corresponding differential cross sections using the phenomenological and semimicroscopic methods of calculation, M3Y-A and KH-A. One can notice that the differential cross sections using the phenomenological and microscopic methods give the same quality of fit with the experimental data. The real phenomenological potential has a smaller range than the folded potentials. The results lead to the necessity of the same renormalization factor N_R in describing the elastic angular distribution as shown in Table IV. At 62 MeV/nucleon, the total reaction cross sections obtained for the M3Y and KH interactions are close to the value ($\sigma_R \sim 361$ mb) in Ref. [12], and that of Moon *et al.* ($\sigma_R = 388$ mb) [3]. One can see that the σ_R for the KH interaction is relatively smaller than that for the M3Y interaction. The similarity between the M3Y and KH interactions at 62 MeV/nucleon is also found at the other two energies, 68.4 and 75 MeV/nucleon, for both the folded potential and the corresponding cross sections.

TABLE V. Parameters of volume and surface imaginary and spin-orbit potentials.

Energy (MeV/nucleon)	r_v (fm)	a_v (fm)	r_s (fm)	a_s (fm)	r_{so} (fm)	a_{so} (fm)
62	0.99	0.70	0.99	0.70	0.54	0.36
68.4	0.99	0.70	0.99	0.70	0.54	0.40
75	0.99	0.70	0.99	0.70	0.54	0.52

D. Effect of using different forms of imaginary optical potentials

The importance of the surface imaginary potential is tested in Fig. 5. The elastic ^{11}Li + p scattering cross section at energy

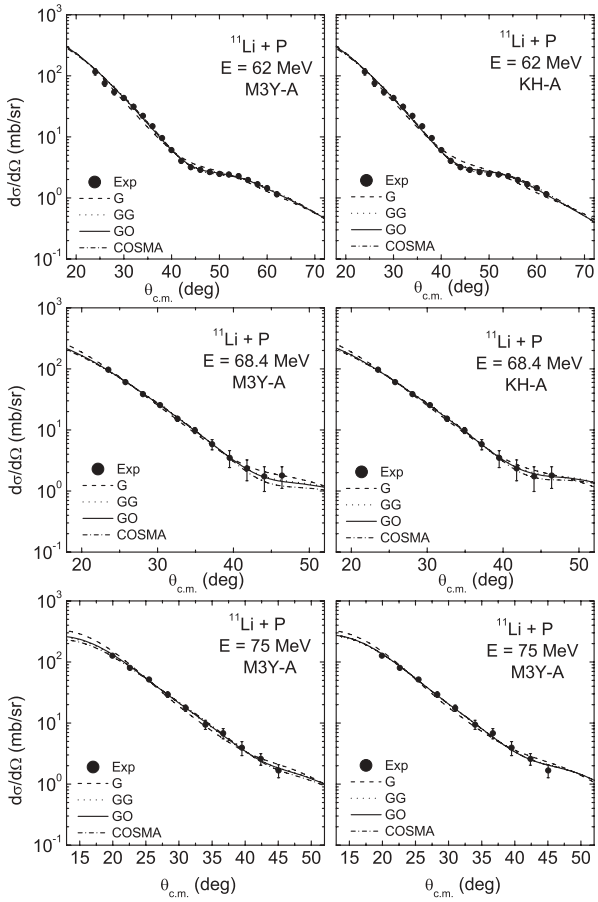

FIG. 3. Elastic ^{11}Li + p scattering cross sections calculated using M3Y-A and KH-A potentials with the four densities for the three energies studied.

$E = 62$ MeV/nucleon, for example, are calculated using M3Y-A potential with GO density with and without the surface imaginary term. It is shown that the surface term is effective on the differential cross section at large angles ($\theta_{\text{c.m.}} > 50^\circ$).

The elastic ^{11}Li + p cross sections using M3Y and KH effective NN interactions with GO density at the energies 62, 68.4, and 75 MeV/nucleon using three methods of calculating OP [(A), (B), and (C)] are presented in Fig. 6. Table VI gives the values of the renormalization factors N_R, N_{IV}, and N_{IS} and the phenomenological optical potential strengths W_v, W_s, and V_{so} obtained by fitting the experimental data for the three types of imaginary potentials with the two interactions using GO density. The results of the renormalization factors are $N_R \sim 0.55$–0.65 for the real folded potentials, $N_{\text{IV}} \sim 0.11$–0.20 for the volume imaginary potentials, and $N_{\text{IS}} \sim 0.01$–0.04 for the surface imaginary potentials. One notices that both N_{IS} and W_s decrease with increasing energy where the projectile protons are more penetrated, so the surface absorption decreases as in normal nuclei. This result is in agreement with that found in Refs. [6,7]. At 62 MeV/nucleon, $N_{\text{IS}} = 0.04$ is close to the value for ^{11}Li + ^{12}C at 60 MeV/nucleon, which equals 0.05 [38]. The imaginary potential decreases as the energy increases and the most decrease is at 75 MeV/nucleon; this is mentioned in previous studies of halo nuclei elastic scattering where the reduction factor of the microscopic imaginary part of the OP is small and gives good results [6,39]. The strength of the spin-orbit potential V_{so} used with the microscopic imaginary potential [method (C)] is found to be smaller than that used with phenomenological one [method (A)]. In general, we found that the three methods give good results. But, we notice from Fig. 6 and the values of χ^2 in Table VI that using OP's calculated in microscopic form with only three free parameters (N_R, N_{IV}, and N_{IS}) and a minimal number of fitting

TABLE VI. Values of the optical potential parameters W_v, W_v, and V_{so}, the renormalization parameters N_R, N_{IV}, and N_{IS}, and the reaction cross sections, obtained by fitting the experimental data for the elastic ^{11}Li + p cross sections at the energies 62, 68.4, and 75 MeV/nucleon using three methods of calculations (see II E for these methods). The folded potential is calculated with M3Y and KH effective NN interactions and the GO density; the other parameters of phenomenological potentials are given in Table V.

Energy (MeV/nucleon)	Pot.	Case	N_R	N_{IV}	N_{IS}	W_v (MeV)	W_s (MeV)	V_{so} (MeV)	σ_R (mb)	χ^2
62	M3Y	A	0.65			13.2	3.7	9.6	362.2	0.75
		B	0.66	0.20			3.2	8.0	354.4	0.85
		C	0.67	0.20	0.04			6.7	364.4	1.09
	KH	A	0.65			13.6	3.2	8.9	353.1	1.18
		B	0.67	0.17			2.9	7.0	329.3	1.14
		C	0.68	0.17	0.04			6.3	351.6	2.23
68.4	M3Y	A	0.56			12.0	2.6	6.0	304.1	0.16
		B	0.59	0.20			2.3	5.6	307.4	0.09
		C	0.61	0.20	0.03			4.9	314.0	0.10
	KH	A	0.57			12.5	2.2	6.0	298.4	0.11
		B	0.59	0.14			2.2	5.1	262.2	0.11
		C	0.60	0.14	0.03			5.1	272.7	0.18
75	M3Y	A	0.54			7.2	1.5	5.5	201.0	0.14
		B	0.55	0.16			0.9	5.4	211.4	0.20
		C	0.55	0.16	0.01			5.1	205.4	0.22
	KH	A	0.55			7.0	1.1	5.4	187.1	0.28
		B	0.55	0.11			0.8	5.1	166.4	0.34
		C	0.55	0.11	0.01			5.1	164.4	0.42

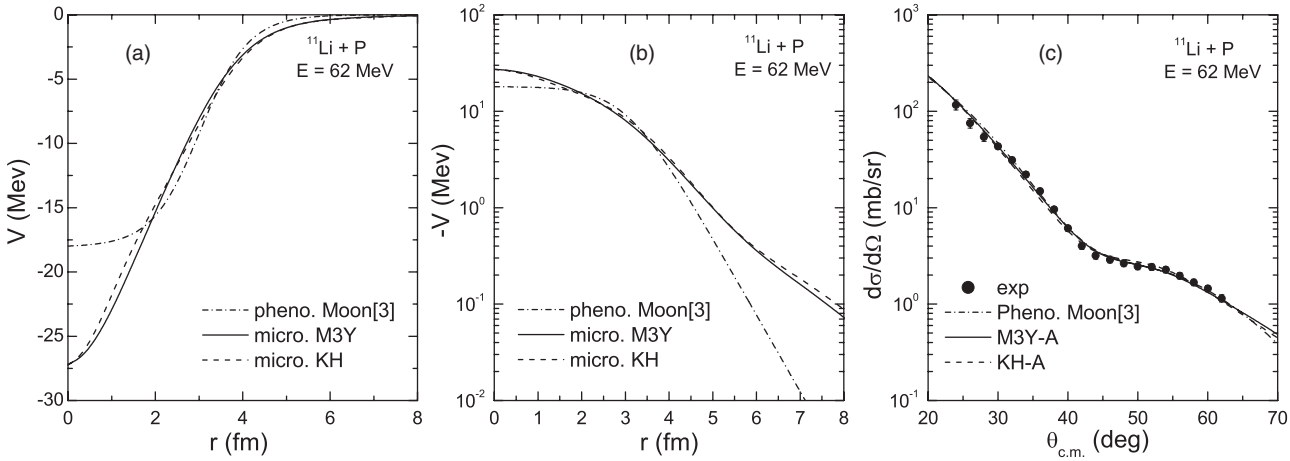

FIG. 4. Real ^{11}Li + p optical potentials at energy $E = 62$ MeV/nucleon using the Woods-Saxon phenomenological form [3] and the folding potential using M3Y and KH interactions with the GO density, shown in (a) linear form and (b) logarithmic scale. (c) Corresponding differential cross sections.

parameters gives good agreement with the available data. Thus, it is not necessary to introduce the large number of arbitrary fitting parameters that were used in the phenomenological and semimicroscopic OP's.

Also, the total reaction cross sections σ_R are listed in Table VI. One can find that the change of the values of σ_R for the different forms of the imaginary potentials does not exceed 10%. Moreover, the total reaction cross sections for the KH interaction are slightly smaller than those for the M3Y interaction, and they decrease with increasing projectile incident energy.

The relation between the renormalization factors of real N_R, volume imaginary $N_{\rm IV}$, and surface imaginary $N_{\rm IS}$ are shown in Fig. 7. We fixed N_R, then at any value of $N_{\rm IS}$, the value of $N_{\rm IV}$ is tested to give the smallest χ^2. This procedure is repeated for different values of N_R. We notice from Fig. 7 that $N_{\rm IV}$ decreases linearly with increasing $N_{\rm IS}$, with a slope $\sim$3; this relation is true at different values of N_R.

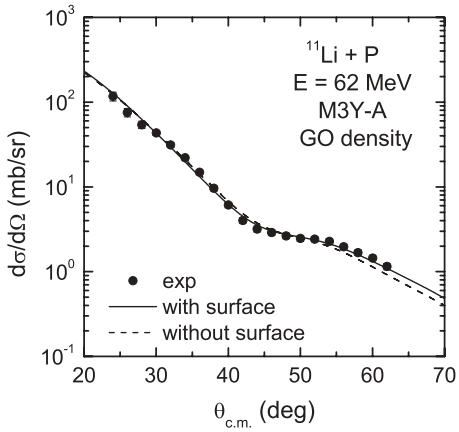

FIG. 5. Elastic ^{11}Li + p scattering cross section at energy $E =$ 62 MeV/nucleon calculated using the M3Y-A potential with and without the surface imaginary term.

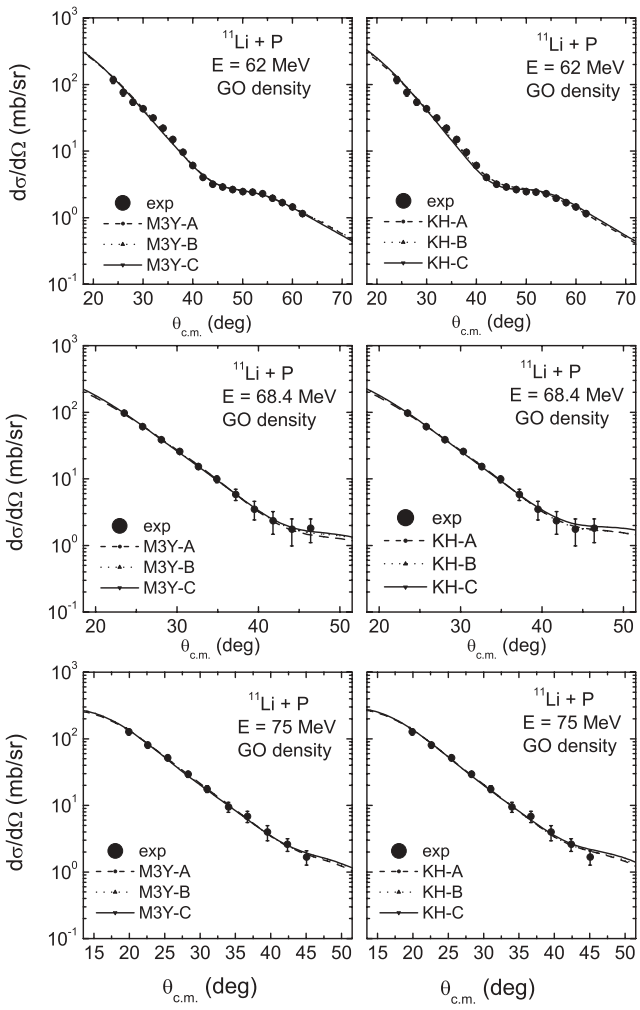

FIG. 6. Elastic ^{11}Li + p scattering cross sections calculated at the energies 62, 68.4, and 75 MeV/nucleon using methods (A), (B), and (C) for calculating the total OP (see II E for these methods). The folded potential is calculated with M3Y and KH effective NN interactions and the GO density.

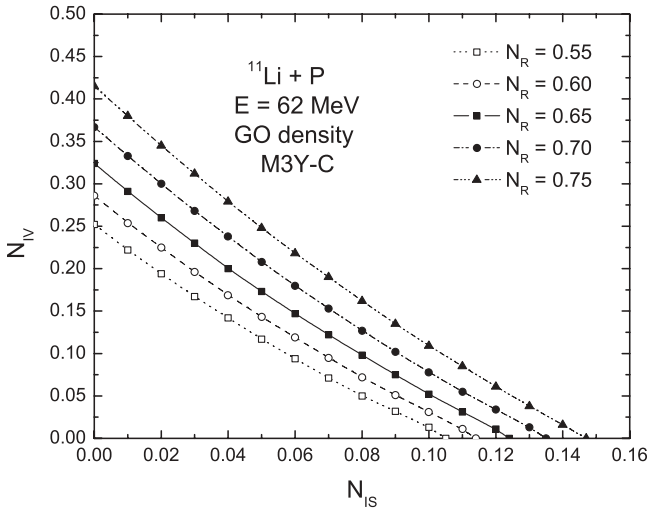

FIG. 7. Relation between the renormalization factors of the volume and surface microscopic imaginary potentials.

The imaginary $^{11}\mathrm{Li} + p$ optical potentials at 62 MeV/nucleon are presented in Fig. 8(a) using the Woods-Saxon form (dash-dotted line) Ref. [3] and the microscopic form using M3Y (solid line) and KH (dashed line) interactions with GO density. (The renormalization factors N_{IV} and N_{IS} of these interactions are listed in Table VI.) The corresponding differential cross sections using the phenomenological method and microscopic method (C) of calculation are shown in Fig. 8(b). The results indicate that

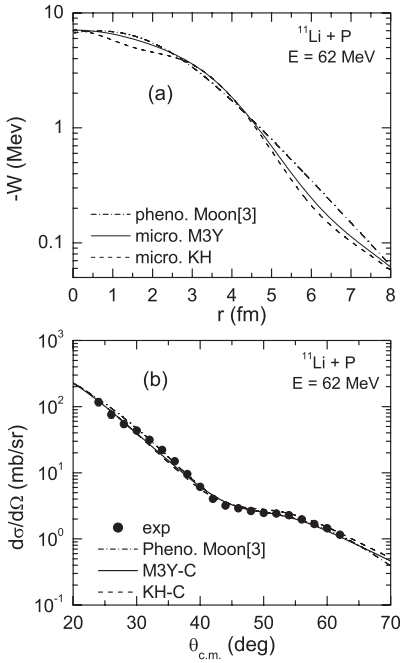

FIG. 8. (a) Imaginary $^{11}\mathrm{Li} + p$ optical potentials at $E =$ 62 MeV/nucleon using Woods-Saxon form (dash-dotted line) in Ref. [3] and the microscopic form using M3Y (solid line) and KH (dashed line) interactions with GO density. (b) Corresponding differential cross sections calculated using the phenomenological method and microscopic method (C).

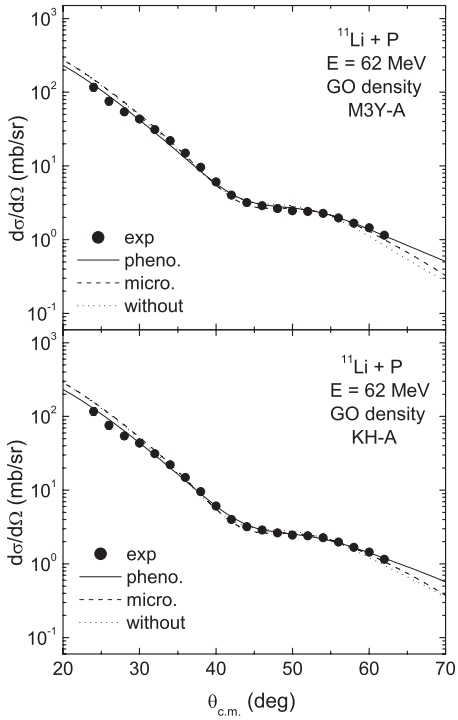

FIG. 9. Elastic $^{11}\mathrm{Li} + p$ scattering cross section at $E =$ 62 MeV/nucleon calculated using M3Y-A and KH-A potentials with GO density with the Woods-Saxon and microscopic forms and without the spin-orbit term.

the imaginary potentials must have a long range to give a good description of the data.

E. Effect of the shape of spin-orbit potential

The effect of the spin-orbit interaction on the cross sections of $^{11}\mathrm{Li} + p$ elastic scattering, using real folded potential and phenomenological imaginary potential with M3Y and KH NN interactions and GO density, is presented in Fig. 9. The solid lines show the results using Woods-Saxon form of the spin-orbit term [see Eq. (28)], while the dashed lines show those using the microscopic form as in Eq. (31); the dotted lines show the results without using the spin-orbit term. We notice that the Woods-Saxon form gives very good fitting with experimental data and is only slightly better than the results obtained with the microscopic form and those obtained without using the spin-orbit term, both of which also give accepted results with both M3Y and KH NN interactions. The results differ slightly at large angles ($>60^\circ$). So the effect of the shape of the spin-orbit term is not strong. This result agrees with that obtained in Refs. [6,39].

IV. CONCLUSIONS

The optical potentials and cross sections of $^{11}\mathrm{Li} + p$ elastic scattering are calculated at three energies (62, 68.4, and 75 MeV/nucleon) within the framework of the single folding model. The real part of the optical potential is constructed by folding two different nucleon-nucleon interactions, namely, M3Y and KH, with ^{11}Li density, which is assumed to be

composed of two parts: a ^{9}Li core and two halo neutrons. Different types of density distributions (G, GG, GO, and COSMA) are used. The density-dependent term is introduced in the folding potentials, whose parameters are adjusted to fulfill the saturation of nuclear matter. The microscopic potentials are constructed from both the renormalized folded potentials and their derivatives. The renormalization factors N_R, $N_{\rm IV}$, and $N_{\rm IS}$ for the real, volume imaginary, and surface imaginary microscopic potentials, respectively, are introduced. Three different forms of imaginary potential are used. These are obtained from combinations of Woods-Saxon and microscopic forms.

The results of the calculations of ^{11}Li + p elastic scattering show that the G density gives accepted fit with data in this work, whereas in previous studies [16,17,31], it does not fit the data for the considered reaction at high energy using Glauber theory. The GG and GO densities obtained from analyzing the measured ^{11}Li + p elastic scattering cross sections, using Glauber multiple scattering theory at high energies, give good results with our work at energies below 100 MeV/nucleon in the framework of the folding model. The form of the density of the two valence neutrons has a small effect on the obtained cross sections.

The obtained renormalization factor of the real folding potential N_R decreases from ∼0.65 to 0.55 with increasing incident energy for both interactions. This value of N_R gives an estimation of the breakup channel effects on the elastic scattering channel.

The renormalization factors (N_R, $N_{\rm IV}$, and $N_{\rm IS}$), the phenomenological parameters (W_s and $V_{\rm so}$), the volume integrals, and the rms radii of the folded potentials are slightly energy dependent.

The shapes of both imaginary and spin-orbit potentials do not play a significant role in describing the considered nuclear reaction. The strength of the spin-orbit potential $V_{\rm so}$ used with the microscopic imaginary potential was found to be smaller than that used with phenomenological one.

The real and imaginary microscopic potentials using only three free parameters N_R, $N_{\rm IV}$, and $N_{\rm IS}$ give results of the same quality as phenomenological potentials with more free parameters. There are two advantages in our work. First, we have only a few fitting parameters, so it is not necessary to introduce the large number of arbitrary fitting parameters used in the phenomenological and semimicroscopic OP's. Second, the microscopic study gives information about the structure, whereas the phenomenological potential is a generalized description and does not include any structure information of the interacting nuclei.

The renormalization factor of microscopic surface imaginary potentials decreases with increasing energy; it has the value $N_{\rm IS} \sim 0.01$–0.04. An interesting linear relation was found between $N_{\rm IV}$ and $N_{\rm IS}$ at constant N_R, namely, $N_{\rm IV}$ decreases linearly with an increase of $N_{\rm IS}$ with slope ∼3 for the three energies.

A comparative study of the two interactions, M3Y and KH, for ^{11}Li + p elastic scattering reveals that the KH interaction, which has no singularity, leads to as good an agreement with the data as the famous M3Y interaction. The two interactions show the necessity of the same renormalization factor N_R. Also, the reaction cross section for the KH interaction is relatively smaller than that for the M3Y interaction. The reaction cross section decreases as energy increases, and these results are close to those of previous work [3,12].

[1] I. Tanihata, J. Phys. G: Nucl. Part. Phys. **22**, 157 (1996).
[2] I. Tanihata, D. Hirata, T. Kobayashi, S. Shimoura, K. Sugimoto, and H. Toki, Phys. Lett. **B289**, 261 (1992).
[3] C. B. Moon, M. Fujimaki, S. Hirenzaki, N. Inabe, K. Katori, J. C. Kim, Y. K. Kim, T. Kobayashi, T. Kubo, H. Kumagai, S. Shimoura, T. Suzuki, and I. Tanihata, Phys. Lett. **B297**, 39 (1992).
[4] A. A. Korsheninnikov, E. A. Kuzmin, E. Yu. Nikolskii, O. V. Bochkarev, S. Fukuda, S. A. Goncharov, S. Ito, T. Kobayashi, S. Momota, B. G. Novatskii, A. A. Ogloblin, A. Ozawa, V. Pribora, I. Tanihata, and K. Yoshida, Phys. Rev. Lett. **78**, 2317 (1997).
[5] A. A. Korsheninnikov, E. Yu. Nikolskii, T. Kobayashi, A. Ozawa, S. Fukuda, E. A. Kuzmin, S. Momota, B. G. Novatskii, A. A. Ogloblin, V. Pribora, I. Tanihata, and K. Yoshida, Phys. Rev. C **53**, R537 (1996).
[6] D. Gupta, C. Samanta, and R. Kanungo, Nucl. Phys. **A674**, 77 (2000).
[7] R. Kanungo and C. Samanta, Nucl. Phys. **A617**, 265 (1997).
[8] A. A. Korsheninnikov *et al.*, Nucl. Phys. **A616**, 189c (1997).
[9] M. D. Cortina-Gil, P. Roussel-Chomaz, N. Alamanos, J. Barrette, W. Mittig, F. S. Dietrich, F. Auger, Y. Blumenfeld, J. M. Casandjian, M. Chartier, V. Fekou Youmbi, B. Fernandez, N. Frascaria, A. Gillibert, H. Laurent, A. Lépine-Szily, N. A. Orr, J. A. Scarpaci, J. L. Sida, and T. Suomijärvie, Phys. Lett. **B401**, 9 (1997).
[10] R. Crespo, Nucl. Phys. **A701**, 429c (2002).
[11] M. Kohno, Phys. Rev. C **48**, 3122 (1993).
[12] A. K. Chaudhuri, Phys. Rev. C **49**, 1603 (1994).
[13] Y. Suzuki, K. Yabana, and Y. Ogawa, Phys. Rev. C **47**, 1317 (1993).
[14] A. A. Korsheninnikov, E. Yu. Nikolskii, C. A. Bertulani, S. Fukuda, T. Kobayashi, E. A. Kuzmin, S. Momota, B. G. Novatskii, A. A. Ogloblin, A. Ozawa, V. Pribora, I. Tanihata, and K. Yoshida, Nucl. Phys. **A617**, 45 (1997).
[15] Y. J. Kim, Int. J. Mod. Phys. E **10**, 91 (2001).
[16] P. Egelhof, Nucl. Phys. **A722**, 254 (2003).
[17] A. V. Dobrovolsky *et al.*, Nucl. Phys. **A766**, 1 (2006).
[18] A. N. F. Aleixo, C. A. Bertulani, and M. S. Hussein, Phys. Rev. C **43**, 2722 (1991).
[19] R. Crespo, J. A. Tostevin, and I. J. Thompson, Phys. Rev. C **54**, 1867 (1996).
[20] A. K. Kerman, H. McManus, and R. M. Thaler, Ann. Phys. (NY) **8**, 551 (1959).
[21] R. Crespo and R. C. Johnson, Phys. Rev. C **60**, 034007 (1999).
[22] Y. Ogawa, K. Yabana, and Y. Suzuki, Nucl. Phys. **A543**, 722 (1992).
[23] D. N. Basu, J. Phys. G: Nucl. Part. Phys. **30**, B7 (2004); Int. J. Mod. Phys. E **14**, 739 (2005).

[24] G. R. Satchler and W. G. Love, Phys. Rep. **55**, 183 (1979).
[25] G. F. Bertsch, J. Borysowicz, H. Mcmanus, and W. G. Love, Nucl. Phys. **A284**, 399 (1977).
[26] D. T. Khoa and G. R. Satchler, Nucl. Phys. **A668**, 3 (2000).
[27] O. M. Knyazov and E. F. Hefter, Z. Phys. A **301**, 277 (1981).
[28] M. El-Azab Farid and M. A. Hassanain, Nucl. Phys. **A697**, 183 (2002).
[29] M. V. Zhukov, B. V. Danilin, D. V. Fedorov, J. M. Bang, I. J. Thompson, and J. S. Vaagen, Phys. Rep. **231**, 151 (1993).
[30] G. Baur and S. Typel, Prog. Part. Nucl. Phys. **59**, 122 (2007).
[31] M. P. Bush, J. S. Al-Khalili, J. A. Tostevin, and R. C. Johnson, Phys. Rev. C **53**, 3009 (1996).
[32] I. Tanihata, T. Kobayashi, O. Yamakawa, S. Shimoura, K. Ekuni, K. Sugimoto, N. Takahashi, T. Shimoda, and H. Sato, Phys. Lett. **B206**, 592 (1988).
[33] G. D. Alkhazov *et al*., Nucl. Phys. **A712**, 269 (2002).
[34] M. E. Brandan and G. R. Satchler, Phys. Rep. **285**, 143 (1997).
[35] M. Y. H. Farag and M. Y. M. Hassan, Czech. J. Phys. **53**, 473 (2003).
[36] R. L. Varner, W. J. Thompson, T. L. McAbee, E. J. Ludwig, and T. B. Clegg, Phys. Rep. **201**, 57 (1991).
[37] K. V. Lukyanov, I. N. Kukhtina, V. K. Lukyanov, Yu. E. Penionzhkevich, Yu. G. Sobolev, and E. V. Zemlyanaya, AIP Conf. Proc. **912**, 170 (2007).
[38] S. A. Fayans, O. M. Knyazkov, I. N. Kuchtina, Yu. E. Penionzhkevich, and N. K. Skobelev, Phys. Lett. **B357**, 509 (1995).
[39] K. V. Lukyanov, V. K. Lukyanov, E. V. Zemlyanaya, A. N. Antonov, and M. K. Gaidarov, Eur. Phys. J. A **33**, 389 (2007).